Davis, M., Matmon, A., Fink, D., Ron, H., Niedermann, S. (2011): Dating Pliocene lacustrine sediments in the central Jordan Valley, Israel – Implications for cosmogenic burial dating. - Earth and Planetary Science Letters, 305, 3-4, 317-327

DOI: 10.1016/j.epsl.2011.03.003

Dating Pliocene lacustrine sediments in the central Jordan Valley, Israel – Implications for cosmogenic burial dating

Davis, M [a]., Matmon, A [a]., Fink, D [b]., Ron, H [a]., Niedermann, S.[c]

[a] The Institute of Earth Sciences, Hebrew University of Jerusalem, Givat Ram, Jerusalem 91904, Israel

[b] Institute for Environmental Research, Australian Nuclear Science and Technology Organization, PMB 1, Menai, NSW 2234, Australia

[c] Helmholtz-Zentrum Potsdam - Deutsches GeoForschungsZentrum, Telegrafenberg, D-14473 Potsdam, Germany

Abstract

Cosmogenic burial dating of sediments is usually used at sites with relatively simple or known exposure-burial histories, such as in caves. In an attempt to extend the applicability of the method to other common geological settings (i.e the dating of late Neogene sedimentary formations), where much less is known about the exposure-burial history, we apply the cosmogenic burial method on Pliocene-early Pleistocene (1.5-4.5 Ma) lacustrine sediments in the central Jordan Valley, Israel. ^{26}Al, ^{10}Be, and ^{21}Ne concentrations in quartz were obtained from a 170 m tectonically-tilted section. Assuming fast burial and no post-burial production we obtained burial ages which range between 3.5 and 5.3 Ma. Integrating simple geological reasoning and the cosmogenic nuclide data, post burial production is found to be insignificant. We also found that the samples contain two distinct populations of grains (chert and quartz) from two different sources which experienced different pre-burial exposure histories. The cosmogenic nuclide concentrations in the samples are in accordance with those expected for the mixing of two sources, and the burial ages computed for both end members agree. Theoretical calculations of two-source mixing show that initial $^{26}Al/^{10}Be$ ratios are depressed relative to the expected surface ratios and may result in burial ages overestimated by as much as 500 ka. Using ages derived from cosmogenic nuclides, independent age constraints, and magnetostratigraphy we correlate the bottom of the section to the Cochiti Normal magnetic subchron (4.19-4.30 Ma) within the Reverse Gilbert chron, and the top of the section to the Reverse subchron at the top of the Gilbert chron (3.60-4.19 Ma).

Introduction

Absolute dating of Plio-Pleistocene continental sedimentary deposits in the age range of 0.5-5 Ma is difficult due to the limited range of radiocarbon (^{14}C), U-series, luminescence (OSL and TL), and Electron Spin Resonance (ESR) dating methods, especially when appropriate material for Ar/Ar dating is not present. This poses a problem in the research of hominid evolution, geomorphology, neotectonics, and late Neogene geology. Stratigraphic relationships and paleontological data usually yield limited results and in many cases, magnetostratigraphic inference has been the only dating tool that provided age constraints to many Plio-Pleistocene continental sedimentary sequences (Opdyk and Channell, 1996). However, interpretation of magnetostratigraphic sequences is often non-unique, unless the sequence can be anchored to one or more absolute age data points. Over the past two decades in-situ produced cosmogenic nuclides have been used in many studies to date burial ages of sediments (0.5-5 Ma) (Granger, 2006). This dating method relies on the in-situ production of cosmogenic nuclides (^{10}Be, ^{26}Al, and stable ^{21}Ne) in quartz initially exposed at the earth's surface and their differential decay during subsequent burial to depths where complete shielding prevents further production. Klein et al. (1986) compared measured ^{26}Al/^{10}Be ratios in Libyan Desert glass to that predicted in non-buried surface rocks to conclude a complex cyclic history of burial and re-exposure of the glass within Libyan sand dunes. In principle, the appearance of ^{26}Al/^{10}Be ratios below the value determined by their surface production rate ratio suggests a period of either complete or partial burial, for example by ice or sediment (e.g. Bierman et al., 1999; Matmon et al., 2003). Numerous geomorphic studies of both surface and buried sediments have demonstrated the wide applicability of the technique. Caves containing fluvial sediments are readily amenable to burial dating since they provide an ideal setting where repeated burial episodes, variation in shielding depth and final re-exposure are absent (Granger et al., 1997; Granger et al., 2001; Haeuselmann et al., 2007; Stock et al., 2004). These studies provide long-term river incision rates by the burial dating of stream deposits in abandoned caves above the modern channel. Burial dating of gravels in cave deposits associated with hominid sites has recently become a powerful chronological tool (Carbonell et al., 2008; Chazan et al., 2008; Gibbon et al., 2009; Partridge et al., 2003; Shen et al., 2009). However, in more common sub-aerial sedimentary formations, such as exposed alluvial fans and abandoned river terraces (Anderson et al., 1996; Granger and Smith, 2000; Matmon et al., 2005; Repka et al., 1997; Wolkowinsky and Granger, 2004) , paleosols covered by glacial till (Balco et al., 2005a; Balco et al., 2005b; Balco et al., 2005c), and lacustrine sediments (Kong et al., 2009) the burial and initial exposure history and the source of the sediment are not always well-constrained and offer an added degree of complexity. Some of these studies use ^{10}Be and ^{26}Al depth profiles to deal with post burial production. Few studies deal with sub-aerial units and compare results with independent ages (Balco et al., 2005a; Granger et al., 2006). In this study we present the use of the cosmogenic burial dating method using ^{10}Be, ^{26}Al and ^{21}Ne on the Erk-el-Ahmar (EEA) formation – an intra-rift lacustrine section exposed in the central Jordan Valley, Israel. The results of the cosmogenic nuclide-based age model are interpreted in light of known stratigraphic, paleomagnetic, paleontological, and independent radiometric dating constraints on the age of the EEA section. The validity of our assumptions regarding initial cosmogenic nuclide concentrations prior to burial, burial history, and post burial production are discussed. We also present an analysis of the ^{26}Al and ^{10}Be data based on the identification and characterization of two populations of mineral grains – chert and quartz – that originate from different sources and discuss the influence of such mixing on a simple burial age model.

Theory of cosmogenic burial dating

The most updated and detailed description of the cosmogenic burial dating method has been recently provided by Granger (2006). The method considers the concentration ratio of two cosmogenic nuclides, generally ^{26}Al and ^{10}Be (^{10}Be half life - 1.39 Ma and ^{26}Al half life - 0.705 Ma) in sedimentary quartz grains that were initially exposed and dosed, and then shielded from cosmic radiation. The $^{26}Al/^{10}Be$ ratio during burial is a function of the initial ratio and the burial time. For most cases, the initial $^{26}Al/^{10}Be$ ratio is simply a function of the production rate ratio which is not influenced by changes in production rate itself and is generally not affected by changes in latitude, altitude, and pre-burial dosing time (Brown et al., 1992; Nishiizumi et al., 1989). Once buried and shielded from cosmic radiation, the $^{26}Al/^{10}Be$ ratio will decrease exponentially due the different half lives of the two isotopes (Granger et al., 1997):

$$\frac{N_{26}}{N_{10}} = \left(\frac{N_{26}}{N_{10}}\right)_0 e^{-t_{burial}\left(\frac{1}{\tau_{26}}-\frac{1}{\tau_{10}}\right)} \qquad (1)$$

where N_{26} and N_{10} are the concentrations of ^{26}Al and ^{10}Be in atoms per gram quartz, $(N_{26}/N_{10})_0$ is the initial $^{26}Al/^{10}Be$ ratio at burial, t_{burial} is the time since burial, and τ_{26} and τ_{10} are the mean lives in years of ^{26}Al ($1.02\times10^6 \pm 0.04\times10^6$ yr) (Nishiizumi, 2004) and ^{10}Be ($2.00\times10^6 \pm 0.02\times10^6$ yr) (Chmeleff et al., 2010; Korschinek et al., 2010). The initial concentrations of cosmogenic nuclides in the sediment prior to its burial can be represented as a function of the erosion rate of the source rock:

$$N_0=P/(1/\tau+E\rho/\Lambda) \qquad (2)$$

where P is the local production rate of the cosmogenic nuclide at the surface (atoms/yr per gram quartz), E is the erosion rate (cm/yr), ρ is the density (g/cm^3), Λ is the attenuation length (g/cm^2), and τ is the mean life (yr). Equations 1 and 2 can be solved iteratively to yield the burial age and the source erosion rate (and initial ^{10}Be concentration) (Granger et al., 1997). A good estimate of the burial age can be obtained provided: a) the burial duration is sufficiently long to create a measurable difference (outside analytical errors) in the concentration ratio compared to the ratio for non-buried sediment (this sets a minimum burial age of about 0.2-0.3 Ma), b) the sediment had a sufficient initial dose of cosmogenic isotopes such that the residual cosmogenic nuclide concentration is larger than the sensitivity limit of Accelerator Mass Spectrometry measurement technique (this sets the maximum burial age to about 5-6 Ma) and c) that it was buried quickly (relatively to its total burial history). An additional, but not essential, requirement is that the sample has remained buried deep enough to eliminate exposure to cosmic radiation. Post burial production via spallation by fast neutrons or by muon capture can be estimated and used to correct for the true burial time if the shielding depth has remained constant (Granger and Muzikar, 2001). For old sediments ($>10^6$ yr), even at depths greater than 10 meters of rock overburden, production via muons maybe significant. Calculating burial ages without including post-burial muon production leads to an underestimation of the true burial age.

The use of a third nuclide in the quartz system can provide additional insight into the processes that affected the burial-exposure history of the investigated sediment (e.g. Vermeesch et al., 2010). The analytical methods and identification of the stable cosmogenic nuclide ^{21}Ne in quartz have been developed by Niedermann, (2000), Niedermann et al., (1997), and Niedermann et al., (1994) and the production ratios of ^{21}Ne/^{26}Al and ^{21}Ne/^{10}Be have been determined giving a sea-level high latitude (SLHL) reference production rate for ^{21}Ne ranging between 18.3 and 19.9 atoms/g/yr (Balco and Shuster, 2009a; Goethals et al., 2009; Niedermann et al., 1994; Niedermann, 2000). In recent studies, the concentrations of ^{21}Ne in sediments were measured and have reinforced ^{26}Al/^{10}Be ages (Placzek et al., 2010; Balco and Shuster, 2009b).

The Erk-el-Ahmar study site

The Erk-el-Ahmar (EEA) formation (Horowitz, 1979) is an intra-rift lacustrine unit exposed in the central Jordan Valley, Israel (Fig. 1). The formation consists of clay, silt, very fine sand layers, and a rich assemblage of fresh water mollusks abundant with

Melanopsis and Unio species (Schütt and Ortal, 1993; Tchernov, 1975). Coarser fragments, such as coarse sand grains, pebbles, and boulders are rare. The lack of a coarse sediment component may suggest minor relief along the shores of the lake that deposited the sediments of the EEA formation. The quartz in the sediments is derived both from aeolian deposition on the drainage basin and from erosion of chert outcrops (further detailed in the results and discussion sections). The studied type section is exposed along the western bank of the Jordan River, ~10 km south of the Sea of Galilee, and is tectonically tilted to the east (10°-25°). The base of EEA is not exposed and horizontal lacustrine sediments of Lake Lisan deposited during the last glacial period overlie the formation on a truncated surface (Picard, 1965). In several areas these sediments have been eroded after the retreat of Lake Lisan. The thickness of the exposed section of the EEA Formation is estimated to be at least 200 m. In the vicinity of the study site there are several other isolated outcrops attributed to the EEA formation, which contain mammalian remains and hand tools (e.g. Braun et al., 1991). However, no exposed stratigraphic relation between these EEA outcrops and the sampled EEA section is currently available and significant unconformities may exist. Thus, the correlation between these outcrops remains undetermined.

The age of the EEA formation is constrained by two other well-studied formations. Although there is no exposed contact between the formations, their relative ages and their relation to the EEA formation are firmly based on fauna assemblages, borehole data, and seismic profile data. The Ubeidiya Formation which has been studied extensively and contains hominid remains, tools, and rich fauna (e.g. Bar-Yosef and Goren-Inbar, 1993; Belmaker et al., 2002; Tchernov et al., 1986), has been dated to ca. 1.5 Ma (Martinez-

Navarro et al., 2009; Tchernov, 1987). Its proto type is exposed ~5 km north of the study site and based on marked differences in mollusk assemblages, the EEA formation is considered to be older than the Ubeidiya formation (Tchernov, 1975). Additionally, the Zihor Lake site in southern Israel, which was dated to ~1.6 Ma (Guralnik et al., 2010), has been correlated with the Ubeidiya formation based on identical tool assemblages (Ginat et al., 2003). The formation which underlies the EEA formation is the Cover Basalt formation; vast flood basalts exposed on both sides of the rift valley and also buried in the valley subsurface. The Cover Basalt was recognized in a borehole in the center of the rift valley and in a seismic profile in which the formation is identified beneath the study site at a depth of ~300 m (Inbar et al., 2010; Marcus and Slager, 1985; Rotstein et al., 1992). A considerable number (n=21) of Ar/Ar and K/Ar ages for the top of the Cover Basalt yield an age range between 3.3 and 4.7 Ma (Heimann et al., 1996). Spatially, the ages are oldest near the study site and become younger to the north, indicating a northerly shift of the volcanic activity (Heimann et al., 1996). Six of the measured ages which are within a 15 km radius from the study area, yield a weighted mean age of 4.5±0.2 Ma. This age sets the maximum age limit for the EEA formation.

Earlier age estimates for the EEA formation ranged between the early Pleistocene and late Pliocene (Horowitz, 1989; Picard, 1965; Schulman, 1959; Tchernov, 1975). Tchernov's (1975) estimate for an early Pleistocene age was partly based on early published K-Ar ages of 1.7—2 Ma (Siedner and Horowitz, 1974) for the underlying Cover Basalt which are far younger than the more recent Ar/Ar ages given above. Magnetostratigraphy studies on the EEA formation show a polarity sequence of RNR (R=Reverse polarity; N=Normal polarity). The normal interval was conservatively interpreted to represent the Reunion (2.13-2.15 Ma) or Olduvai (1.78-1.95 Ma) subchrons (Braun et al., 1991; Ron and Levi, 2001). Combining all the above age estimates, the age of EEA formation appears to be constrained between 1.5-4.5 Ma. In order to further constrain the age of the EEA formation we apply the technique of burial dating of these lacustrine sediments from different depths using cosmogenic ^{10}Be, ^{26}Al and ^{21}Ne.

Sample collection and analytical procedures

Eleven samples of silty-fine sand (Fig. 1) were collected from beds within the EEA formation from depths between 2 m to 36 m below the present day erosional surface (8 of the 11 were from >12 m depth; Fig. 1). Samples 1a to 1d were collected from the same stratigraphic horizon and thus are expected to show similar burial ages. However, the geometry imposed by the tilting of the EEA formation and its later truncation positions these samples at decreasing depths below the surface. Deviations from this expectation of coeval age can constrain the changes in post-burial shielding depth and the impact of post burial production of cosmogenic nuclides by muons on the isotopic ratio. Present and ongoing slope processes, mostly the frequent recurrence of small landslides which repeatedly expose fresh sediment, suggest that the sampled section has been exposed only recently after the incision of a side gulley and the meandering of the Jordan River. Thus, we assume that exposure of the sampled section is very recent. To further reduce the possibility of production of cosmogenic isotopes due to recent exposure, samples were collected after removal of an additional ~0.5 m of sediment at the exposed face. All samples were sieved and the >61 μm size fraction was further processed (upper grain size limit – 125-250 μm). Quartz was separated after carbonate dissolution in warm HCl

(18%) and magnetic separation. Quartz was further etched at least twice in a 2.5% HF:1% HNO_3 solution. Extraction of Al and Be followed standard techniques described in Bierman and Caffee (2001). Five samples were analyzed for $^{10}Be/^{9}Be$ and $^{26}Al/^{27}Al$ ratios at the ANTARES Accelerator Mass Spectrometry (AMS) facility at the Australian Nuclear Science and Technology Organization (ANSTO) (Fink et al., 2004; Fink and Smith, 2007); 6 additional samples were analyzed at the Lawrence Livermore National Laboratory (LLNL) (Rood et al., 2010). Two samples were analyzed for ^{21}Ne at Deutsches GeoForschungsZentrum (GFZ) in Potsdam (Niedermann et al., 1997). Noble gases were extracted from the quartz samples both by crushing and stepwise heating, in order to characterize the compositions of both the trapped gases contained in fluid inclusions and the lattice-bound gases (including the cosmogenic component), respectively. For crushing, ~1 g of quartz was loaded into an ultra-high vacuum crusher and then baked for 24 hours at 100°C before gas extraction. For stepwise heating, the samples were ground to a grain size of ~100 µm before being wrapped in Al foil and loaded in the sample carrousel above the extraction furnace, which was then baked at 100°C for about one week, and noble gas extraction was achieved in four heating steps of 400, 600, 800, and 1200°C for at least 20 minutes each. Chemically active gases were removed on two Ti sponge and two SAES (ZrAl) getters. He, Ne, and Ar-Kr-Xe were separated from each other by trapping in a cryogenic adsorber and subsequent sequential release. Noble gas concentrations and isotopic compositions were determined in a VG5400 sector field mass spectrometer, and were corrected for isobaric interferences, instrumental mass fractionation, and analytical blanks.

To enable the comparison of all $^{10}Be/^{9}Be$ data, ratios were normalized to a self consistent pair of standard reference materials at both ANSTO and LLNL based on nominal values of 2.790×10^{-11} for NIST SRM-4325 and 2.851×10^{-12} for 07KNSTD3110, respectively. Similarly, all $^{26}Al/^{27}Al$ ratios were normalized to a self consistent pair of SRMs with nominal values of 1.680×10^{-11} for Vogt SRM Z93-0221 and 1.065×10^{-11} for KNSTD 10650 (see table 2 and 3 in Fink and Smith, 2007; Nishiizumi, 2004; Nishiizumi et al., 2007). Scaling factors for spallation for all measured samples were calculated using methods described in Dunai (2000). Correspondingly, SLHL total production rates for ^{10}Be and ^{26}Al in quartz are 4.55 ± 0.52, 31.0 ± 3.5 atoms g^{-1} yr^{-1}, respectively (Dunai, 2000). The spallation production values are from Balco et al. (2008) and updated at http://hess.ess.washington.edu. The muon production values are from Granger and Smith (2000 and references therein). SLHL production rate of 18.3 ± 0.5 atoms g^{-1} yr^{-1} for ^{21}Ne in quartz is taken from Balco and Shuster (2009a). Balco and Shuster (2009a) ^{21}Ne production calculations used the scaling of stone (2000) which in this case is similar to Dunai (2000) as there is no latitude scaling (>60°) for the calibration site and the air pressure scaling is similar for both methods. Goethals et al. (2009) have shown that common calibration-curve-analysis of ICP-OES measurements of stable Al may underestimate Al concentrations by 7-11% compared to the standard addition method. Thus, these authors further discuss that total reference ^{26}Al production rates may be higher, ~35.7 atoms g^{-1} yr^{-1}. Until this is resolved we continue to use the published values of ^{26}Al production rates (e.g. Balco et al., 2008). A source rock density of 2.65 g/cm^3 and an attenuation length of 160 g/cm^2 (Gosse and Phillips, 2001) were used. Attenuation parameters for muons were taken from Granger and Muzikar (2001) and pre-burial concentrations were calculated assuming steady erosion of the source basin via equation 2 (Granger and Muzikar, 2001).

Observation of sample grains under the microscope revealed two distinct grain populations: quartz and chert. As both grain types are common in size, density and magnetic properties, we were unable to physically separate between them. Nevertheless, they are visually distinguishable. Thus, the proportion between quartz and chert in each sample was determined by grain counting. Grain counting was carried out by preparing 2 or 3 small aliquots per sample of sediment, and then taking 2-3 photos per aliquot which were then individually counted under magnification. Chert/quartz ratios were combined with the cosmogenic data to elucidate pre-burial processes.

Results

Cosmogenic data

^{10}Be concentrations of all samples are on the order of 10^5 atoms/g quartz, with ~3% analytical uncertainties (Table 1; all uncertainties are 1σ). ^{26}Al concentrations are usually less than 10^5 atoms/g quartz with large uncertainties for 5 of the 12 samples (~ 40-50%) due to the high AMS measurement uncertainty close to the detection limit. For two samples (EEA-1b and EEA-2) cosmogenic ^{21}Ne concentrations range between 52×10^5 atoms/g quartz and 54×10^5 atoms/g quartz. To determine the concentrations of cosmogenic ^{21}Ne, the data were first plotted on a three-isotope diagram (Fig. 2). In such a plot, data aligned along the “spallation line” indicate two-component mixtures between atmospheric and cosmogenic Ne (Niedermann et al., 1993), whereas deviations from that line may imply the presence of additional components, such as nucleogenic Ne produced by the reactions $^{18}O(\alpha,n)^{21}Ne$ and $^{19}F(\alpha,n)^{22}Na(\beta^{+})^{22}Ne$, where α particles are derived from U and Th decay. A nucleogenic component typically shows up most clearly in the 1200°C heating step, in which no cosmogenic Ne is released any more (Niedermann, 2002). For samples EEA-1B and EEA-2, the 400-800°C data plot generally along the spallation line; small deviations (as for EEA-2 600°C) can be explained by slight isotope fractionation. The crushing data are consistent with the atmospheric composition within uncertainties. However, ~23-28% of the total ^{21}Ne excesses are degassed in the 1200°C steps, indicating a substantial contribution of nucleogenic Ne in these samples; for EEA-1B this assumption is further supported by the position of the 1200°C data point well off the spallation line. Therefore, while the 400 and 600°C steps can be regarded to represent simple mixtures of atmospheric and cosmogenic Ne, the 800°C steps probably include some nucleogenic Ne. Therefore, the total cosmogenic ^{21}Ne concentration for each sample was calculated as the sum of the ^{21}Ne excesses (relative to atmospheric composition) in the 400 and 600°C steps, added by (50±50)% of that in the 800°C step, as shown in Table 2.

Cosmogenic burial ages for the EEA formation are initially computed assuming no post burial production of cosmogenic nuclides. The justification for this assumption is discussed below. The measured $^{26}Al/^{10}Be$ ratios in EEA samples are very low (<0.95) (Table 1). These ratios correspond to burial ages that range between 3.6 and 5.3 Ma (Table 3; Fig. 3), close to the limit of the method. Sample EEA-3 with a measured $^{26}Al/^{10}Be$ concentration ratio of 0.05 +/- 0.05 plots in the “forbidden zone” for in-situ produced ^{26}Al and ^{10}Be in quartz (Fig. 3). Two ^{21}Ne measurements yielded ^{26}Al-^{21}Ne, and

^{10}Be-^{21}Ne ages, which are consistent within 1σ with the corresponding ^{26}Al-^{10}Be ages (Table 3; Fig. 4).

The calculation of a burial age depends on the assumed production rate that existed during the initial dosing of the source bedrock. This is mostly pronounced for samples with initial ^{10}Be concentrations larger than ~10^6 atoms/g as is the case of the EEA samples where exposure ages are the greatest and erosion rates are the slowest. As the early Pliocene landscape in the study area was characterized by low relief close to sea level (Zilberman and Begin, 1997), burial ages were computed assuming initial production at a mean basin altitude of 100 m (Dunai scaling-factor = 0.81). Uncertainties in the rock source altitude and geomagnetic field intensity has a relatively small effect on the age compared with the age uncertainties derived from the analytical uncertainties. For example, a change in mean basin altitude from 100 m to 400 m and a decrease of 30% in the integrated geomagnetic field intensity (i.e a total increase of ~50% in production rates) (Dunai, 2000; Dunai, 2001) is equivalent to an increase of 2-5% in the burial ages.

Grain counting results reveal that the quartz and chert grains mix at different ratios among the samples, and range between 3 and 50% chert content (Fig. 5). ^{10}Be and ^{26}Al concentrations from samples EEA-1 (a to d) to EEA-4 (n=7) show a clear mixing trend between the two grain type end members (Fig. 5B) with ^{10}Be concentrations in the pure chert end member being ~9 times higher than in the pure quartz end member (Fig 3B). ^{26}Al concentrations in chert are ~4 times higher than in quartz. The different mixing ratios most likely reflect the natural variance in mineral ratios within fine alluvial sediment. Furthermore, since our samples are collected from a layer 30 cm thick, which was deposited over hundreds to thousands of years, the variability may also reflect short term temporal variation in mineral ratios. Samples EEA-5, 6, 7a and 9, which are situated further up-section, plot above the ^{10}Be and ^{26}Al mixing lines (Fig. 5B).

Paleomagnetic data

Samples for paleomagnetic directional measurements were collected from five locations within a ~3 m section at the top of the exposed EEA formation. Each location was sampled twice for alternating field demagnetization measurements (AF) and three of the locations were also sampled for thermal demagnetization. Incremental thermal demagnetization experiments from room temperature to 600°C yielded a small, yet stable moderate negative inclination with a SE declination that is interpreted as a primary reverse polarity with a strong normal overprint (95% of the magnetization was removed at 300 C°). Paired samples were subjected to stepwise Alternating Field (AF) demagnetization that yielded a moderate positive direction with northerly declination upon removal of ~95% of the magnetization. Thus, the AF is not sensitive enough to recover the stable primary reverse component of the natural remanent magnetization (NRM). We conclude that the NRM of this part of the section is composed of two vectors, a primary stable reversed component overprinted by a strong normal one. In the discussion section, we add these results to results from previous paleomagnetic studies and compare them to the cosmogenic nuclide burial ages.

Discussion

Geological constraints

The burial ages obtained for the Erk-el-Ahmar formation, assuming a simple exposure and burial history, range between 3.6-5.3 Ma (Table 3 and Fig. 3B). These ages, which approach the age limit of the ^{26}Al-^{10}Be burial dating method, are more than twice as old as previous age estimates (~1.8 Ma). Nevertheless, they are consistent with the maximum age limit constraint set by the Cover Basalt unit (4.5 Ma).

The effect of post burial production of cosmogenic isotopes and depressed initial $^{26}Al/^{10}Be$ ratios on burial ages must be addressed when applying the cosmogenic burial dating method. $^{26}Al/^{10}Be$ ratios at the time of burial which are lower than those predicted by steady surface erosion (i.e. depressed ratios) will cause an overestimation of the burial age (e.g. Granger et al., 2006). Post burial production by muons increases as burial depths decrease and/or burial time increases (e.g. Granger and Muzikar, 2001). Not accounting for post burial production by muons will result in an underestimation of the burial age. There are a few reasons to believe that post burial production is negligible in our study area.

1. $^{26}Al/^{10}Be$ ratios (and thus burial ages) do not show any dependency on the current vertical shielding depths of the samples. Specifically, in samples EEA- 1a to 1d.
2. The ages overlap the maximum age constraint for the EEA formation – the underlying Cover Basalt (~4.5 Ma). Significant post burial production would yield corrected ages older than the Cover Basalt Formation, a situation that is geologically impossible.

Additionally, if we assume that the present shielding depth has been constant over the entire burial time of >4 Ma, post burial production itself would have produced more ^{26}Al than that measured in the samples. This means that shielding had to be much thicker over a considerable length of the total burial time and only recently reduced. Four samples from the same horizon (EEA-1a to EEA-1d) are presently situated at different shielding depths. The comparison between their measured ^{10}Be and ^{26}Al concentrations allows us to constrain the shielding history. If post burial production was significant, sample EEA-1a, the deepest and most shielded of the four samples, should have yielded the lowest ^{10}Be and ^{26}Al concentrations and the shallowest sample, EEA-1d, should have yielded the highest concentration. However, sample EEA-1a, yielded the highest nuclide concentrations and lowest ^{26}Al/^{10}Be ratio. The depth difference between EEA-1a and EEA-1d is 12 m (1920 g/cm^2 for a sediment density of 1.6 g/cm^3). This difference is 1.27 and 0.44 times the attenuation length for negative muons and fast muons, 1510 and 4320 g/cm^2 , respectively (Heisinger et al., 2002a; Heisinger et al., 2002b). This means that at any shielding depth and over any exposure time sample EEA-1a would have experienced a reduction by 35% in post burial production by fast muons compared to sample EEA-1d and a reduction by 75% due to negative muons. These differences are not observed in the samples and the variations in the nuclide concentrations are best explained by chert-quartz mixing (Fig. 5B). The absence of significant post-burial production by muons implies significant shielding that eliminated post burial production for most of the burial time.

Depressed ^{26}Al/^{10}Be ratios may be the result of several processes such as fast erosion of old sediments and their incorporation into the stream network or sediment storage (e.g. Balco et al., 2005a; Bierman and Caffee, 2001). In order to overestimate the burial age of EEA sediments by 2 Ma, for example, sediments would have to be buried at the EEA site with a ^{26}Al/^{10}Be ratio of ~2 (Fig 3A). Although depressed ratios in surface sediments can yield apparent burial ages of >1 Ma (e.g. Kober et al., 2009), usually they will not cause age overestimations of more than 500 ka (e.g. Bierman and Caffee, 2001; Bierman et al., 2005; Kober et al., 2007).

In our case, depressed initial ratios are the result of sediment mixing from two sources with distinctively different pre-burial doses, i.e., paleoerosion rates (Fig. 3A). Such mixing will have an impact only if one of the sediment end members is initially highly dosed (i.e. positioned on the low erosion rate side of the exposure-burial plot). The determination of the mixing ratio can assist in applying the needed correction to eliminate the effect of sediment mixing on the initial $^{26}Al/^{10}Be$ ratio (Fig. 3B). Mixing of sediment most likely occurs in many fluvial systems where sediment is derived from various, and very different, sources. Once mixed, quartz grains from those various sources generally cannot be distinguished, the mixing is not apparent and the mixing ratio cannot be determined. However, the mixing of sediment from different sources in the EEA formation is apparent. Chert and quartz grains are visibly distinguishable (Fig. 5A) and mixing ratios can be determined by grain counting (see methods section). The two grain populations have a different source and exposure history. The chert is derived from weathering of surrounding Eocene and Senonian bedrock outcrops. The quartz is delivered by aeolian processes from a more distant source. Two observations support this assessment: a) paleosols in the vicinity, which are preserved in between Pliocene basalt flows, contain quartz in the silt and fine sand fraction. As there is no quartz present in the basalts, it is considered to be of an aeolian origin (Graef et al., 1997; Singer, 2007); b) there are no quartz sand outcrops which fit the grain sizes in the EEA formation. Thus, the source of quartz in EEA is assumed to be from the erosion of the aeolian input to soils in the drainage basin. If the sources for chert and quartz have each eroded at a different rate or were derived from different altitudes, it is expected that for samples of similar age, cosmogenic nuclide concentrations fall on a simple mixing curve. We test this assumption on samples EEA-1 (a-d) to EEA-4 which originate from a fairly thin sedimentary section (6 m) at the bottom of the exposed sequence (Fig 1C). Late Pleistocene lacustrine sediments in the rift valley accumulated in rates of ~0.7 mm/yr (Haase-Schramm et al., 2004) Assuming a conservative sedimentation rate of 0.2 mm/yr (Sadler, 1981), these samples represent a time span of 3×10^4 years. As this time span is two orders of magnitude shorter than the overall age of the sediments, the assumption of similar age for samples EEA-1 to EEA-4 is a valid one. As expected, ^{10}Be concentrations from these samples show a mixing trend between the two grain type end members with ^{10}Be concentrations in chert being ~9 times higher than in the quartz end member (Fig. 5B). Samples EEA-1(a-d) to EEA-4 (excluding EEA-3) also show a linear mixing of ^{26}Al concentrations with ^{26}Al concentrations in chert being ~4 times higher than in the quartz end member (Fig. 5B). The simple burial age of every sample which contains a mixture of chert and quartz must be corrected for this mixing affect. Only the end members which contain pure chert or quartz can yield a simple burial age that is not affected by sediment mixing. ^{26}Al and ^{10}Be concentrations for quartz and chert end members that are obtained from the best-fit mixing lines for samples EEA-1 to 4 (Fig. 5B) correspond to a burial age of 4.5±0.6 Ma which is the weighted mean of the pure quartz and chert end member ages (Fig. 3B, Table 3).

Therefore, the simple burial ages of samples EEA-1 (a to d) to EEA-4 which range between 4.5 Ma and 5.1 Ma were corrected to 4.5±0.6 Ma by considering sediment mixing (Fig. 3B, Table 3) Similarly, samples EEA-5 and EEA-6 are positioned on a possible mixing curve (with a different slope) and sample EEA-7a and EEA-9 are yet even higher. Their corrected ages were calculated by their distance on exposure-burial plot from the mixing curve of samples EEA-1 (a to d) to EEA-4 (Fig. 3B).

It is important to note that EEA samples closest to represent the end members (sample EEA-2 with <5% chert and sample EEA-5 with ~60% chert) yield similar burial ages (Fig. 3B), thus ruling out the possibility that one of the end members (represented by chert or quartz) was originally buried with a depressed ^{26}Al/^{10}Be ratio. If either the chert or quartz had been buried with a significantly low ^{26}Al/^{10}Be ratio, the calculated ages of these end member samples would have been different from each other. The fact that the two very different sources agree is not obvious because aeolian (dune) material is known to have depressed ^{26}Al/^{10}Be ratios due to multiple cycles of burial-exposure episodes (Klein et al., 1986; Nishiizumi et al., 1993). The quartz in EEA however is fine windblown material which probably resided in surrounding soils and thus experienced longer times of exposure (apposed to dune environments).

The ^{26}Al concentration measured in sample EEA-3 plots well under the mixing line for ^{26}Al (Fig. 5B). In contrast, the ^{10}Be concentration measured in sample EEA-3 does follow the mixing trend (Fig. 5B). Consequently, due to the lower than expected ^{26}Al concentration, this sample is positioned in the “forbidden zone” of the ‘exposure burial plot’ (Fig. 3). This ‘deficiency’ in ^{26}Al may be related to the high chert content in sample EEA-3. Other measurements of cherts in Israel have also yielded lower than expected ^{26}Al/^{10}Be ratios (e.g. Boaretto et al., 2000; Matmon et al., 2003).

^{21}Ne ages for sample EEA-2 (4% chert) are similar within 1σ to its ^{26}Al-^{10}Be age, adding to the validity of the ^{26}Al-^{10}Be age model. In sample EEA-1b (17% chert), ages are also consistent within 1σ, although the mean ages decrease among the different nuclide pairs (^{26}Al-^{10}Be, ^{21}Ne-^{26}Al, ^{21}Ne-^{10}Be, respectively). The slightly different behavior of the above two samples suggests that the age difference in sample EEA-1b is related to its chert content. Balco and Shuster (2009b) have shown a similar decrease in ^{21}Ne-^{26}Al-^{10}Be ages in chert grains from one sample from Riverbluff Cave in Missouri. One possible explanation for the decrease in the age is the underestimation of cosmogenic ^{21}Ne in chert due to diffusion of Ne related to the small crystal structure of chert (Fig. 4 in Shuster and Farley, 2005). Doubling of the ^{21}Ne concentration in sample EEA-1b would yield mean burial ages that agree among all three isotope pairs. Alternatively, the underestimation of ^{26}Al as discussed above may also explain the age decrease.

Correlation with the magnetostratigraphy

In the absence of independent dating, previous interpretation of the paleomagnetic stratigraphy (Braun et al., 1991; Ron and Levi, 2001) followed the most conservative path and correlated the base of the exposed sequence of the EEA formation to the Reunion (2.13-2.14) and Olduvai normal (1.78 - 1.95 Ma) subchrons, respectively. These paleomagnetic studies included broad-brush sampling (Braun et al., 1991) and more high resolution sampling (~10 cm) on a detected reversal boundary in mid-section (Ron and Levi, 2001). The additional samples obtained from the top of the section overlap with cosmogenic nuclide sample EEA-7a and show a reverse polarity. Using geological constraints and our corrected burial ages (Table 3), several correlations to the magnetostratigraphic sequence are possible (Fig. 6). The most probable one correlates the base of the exposed sequence of the EEA formation normal section, which includes samples EEA-1 (a to d) to EEA-6 (Fig. 6), to the Cochiti normal subchron (4.19-4.30 Ma, Lourens et al., 2004; Ogg and Smith, 2004) of the Gilbert chron. This is the oldest normal polarity subchron which post dates the age of the Cover Basalt formation. Cosmogenic nuclide burial ages, geological data, and field observations suggest that the upper part of the EEA formation from which samples EEA-7a and EEA-9 were collected, is significantly younger than the bottom part, from which all other sample were collected. Both the ^{26}Al and ^{10}Be concentrations of samples EEA-7a and EEA-9 plot above the ^{26}Al and ^{10}Be best-fit mixing lines which correlate to an age of ~4.5 Ma (Fig. 5B). The ^{26}Al/^{10}Be ratio of sample EEA-7a (0.55±0.05) corresponds to a burial age of $4.16_{+0.19/-0.18}$ Ma. When corrected for the effect of sediment mixing, the age is reduced to 3.7±0.2 Ma. The ^{26}Al/^{10}Be ratio of sample EEA-9 (0.93±0.07) correlates to a burial age of $3.58_{+0.16/-0.17}$ Ma. When corrected for the effect of sediment mixing, the age is reduced to 3.15±0.17 Ma. As expected, the ages of samples EEA-7a and EEA-9 are younger than the ages obtained for the bottom part of the section; however, their ages are stratigraphically inverted (EEA-9 was collected ~40 m below sample EEA-7a and yields a younger age). The age range given by both samples (3.15-3.7 Ma) includes three reversed subchrons, two of which are short lasting (Fig. 6). The simplest interpretation places EEA-7a and EEA-9 at the beginning of the Gilbert chron (3.60-4.19 Ma). This interpretation is based on the assumption that both samples are within a continuous and single period of reversed polarity and are contained within a section thicker than 85 meters (Fig. 6).

Several field observations support the age gap between the top of the section to the bottom. Sample EEA-7a is positioned ~85 m above sample EEA-6 where the bedding dip is 10°, shallower than at the bottom part (24°). The change in dip from 24° to 10° implies a significant time gap of >10^5 yr that would allow tectonic activity to be so pronounced. Additionally, a thin conglomerate layer outcropping between the two samples suggests an erosional unconformity and a gap in time. Our paleomagnetic interpretation differs significantly from previous interpretations (Braun et al., 1991; Ron and Levi, 2001) that were correlated mainly to palynological data (Horowitz, 1979; Horowitz, 1989). This emphasizes that the strength of a paleomagnetic interpretation is based on the strength of the absolute age anchors, and demonstrates the advantages of dating Pliocene sediments using both cosmogenic nuclides and paleomagnetic methods in concert.

Implication for the formation of the Jordan rift valley

The cosmogenic burial ages for the EEA formation require us to reassess the timing of the formation of the Jordan rift valley as a significant morphotectonic depression. Miocene continental sediments are not restricted to the Jordan rift and were deposited in what is known as the 'northern Israel Neogene basin' (Shaliv, 1991). Although sedimentation rates were much higher in the subsiding rift up to the time of the Cover Basalt, the boundaries of the basin were not solely determined by Jordan rift tectonics (Shaliv, 1991). The EEA sediments are the oldest known sediments confined to the rift valley. This restricted spatial distribution and the fact that the EEA formation appears immediately after the emplacement of the Cover Basalt means that the deposition of the EEA formation in a shallow basin occurred simultaneously to the initial uplift of the Jordan rift margins, the termination of the subsidence and sedimentation in the Neogene basin, and the continued subsidence of the Jordan Valley (within the Dead Sea rift).

The paleo-erosion rates of the chert are extremely low (<0.2 m/Ma) and yield high pre-burial dosing values (~10^7 ^{10}Be atoms/g). These erosion rates are expected for such a durable rock. Matmon et al., (2009) calculated <0.2 m/Ma erosion rates from chert clasts in the low relief hyper arid terrain of the central Negev in Israel. In contrast, chert and silicified carbonate rocks at sites with significant relief in Israel yielded erosion rates 10 times higher (Fruchter, 2009; Haviv, 2006). The low erosion rates and the small grain size distribution in the EEA sediments conform to a low relief environment. This would be the expected topography at the beginning of subsidence after the Cover Basalt filled the previous landscape. Large scale incision and channeling, which occurred later in the history of the rift, would have exposed chert outcrops to boulder detachments and cliff retreat, causing much lower pre-burial dosing.

Conclusions

Cosmogenic burial ages, using ^{26}Al, ^{10}Be, and ^{21}Ne in quartz-chert sedimentary mixtures, were obtained for the lacustrine Erk-el-Ahmar formation in the central Jordan valley, Israel. These ages range between 3.6 and 5.3 Ma (3.15-4.5 Ma corrected ages) and are at the limit of the cosmogenic ^{10}Be-^{26}Al nuclide burial dating method. They are more than twice as old as previous age estimates for the EEA formation, but are consistent with its known geological age constraints. Using age constraints, magnetostratigraphy, and corrections for two-source sediment mixing we conclude a most probable burial age of 4.19-4.30 Ma for the base of the exposed section of the EEA and 3.60-4.19 Ma for the top of the section. The observed mixing of quartz and chert grains from different sources is seen in both ^{26}Al and ^{10}Be concentration trends. We show that source mixing causes initial depressed $^{26}Al/^{10}Be$ ratios, unrelated to other processes such as sediment storage. Detection of the source mixing allowed us to correct cosmogenic burial ages based on the degree of mixing. Source mixing has implications for the burial dating method because usually different sources cannot be distinguished in quartz samples. We conclude that the simple exposure-burial age model assumptions are met, perhaps with some depressed initial $^{26}Al/^{10}Be$ ratios causing a slight overestimation of the age. The ^{21}Ne-^{26}Al and ^{21}Ne-^{10}Be burial ages are lower than the ^{26}Al-^{10}Be age of the sample containing chert. This is attributed to an underestimation of ^{26}Al or ^{21}Ne in chert.

Bibliography

Anderson, R.S., Repka, J.L., Dick, G.S., 1996. Explicit treatment of inheritance in dating depositional surfaces using in situ ^{10}Be and ^{26}Al. Geology 24, 47-51.

Balco, G., Stone, J.O., Jennings, C., 2005a. Dating Plio-Pleistocene glacial sediments using the cosmic-ray-produced radionuclides ^{10}Be and ^{26}Al. American Journal of Science 305, 1-41.

Balco, G., Stone, J.O., Mason, J.A., 2005b. Numerical ages for Plio-Pleistocene glacial sediment sequences by ^{26}Al/^{10}Be dating of quartz in buried paleosols. Earth and Planetary Science Letters 232, 179-191.

Balco, G., Stone, J.O., Rovey, C., 2005c. The First Glacial Maximum in North America. Science 307, 222.

Balco, G., Stone, J.O., Lifton, N.A., Dunai, T.J., 2008. A complete and easily accessible means of calculating surface exposure ages or erosion rates from ^{10}Be and ^{26}Al measurements. Quaternary Geochronology 3, 174-195.

Balco, G., Shuster, D.L., 2009a. Production rate of cosmogenic ^{21}Ne in quartz estimated from ^{10}Be, ^{26}Al, and ^{21}Ne concentrations in slowly eroding Antarctic bedrock surfaces. Earth and Planetary Science Letters 281, 48-58.

Balco, G., Shuster, D.L., 2009b. ^{26}Al-^{10}Be-^{21}Ne burial dating. Earth and Planetary Science Letters 286, 570-575.

Bar-Yosef, O., Goren-Inbar, N., 1993. The Lithic Assemblages of ‘Ubeidiya, a Lower Paleolithic Site in the Jordan Valley. The Institute of Archaeology, The Hebrew University of Jerusalem, Jerusalem.

Belmaker, M., Tchernov, E., Condemi, S., Bar-Yosef, O., 2002. New evidence for hominid presence in the Lower Pleistocene of the Southern Levant. Journal of Human Evolution 43, 43-56.

Bierman, P.R., Marsella, K.A., Patterson, C., Davis, P.T., Caffee, M., 1999. Mid-Pleistocene cosmogenic minimum-age limits for pre-Wisconsinan glacial surfaces in southwestern Minnesota and southern Baffin Island; a multiple nuclide approach. Geomorphology 27, 25-39.

Bierman, P.R., Caffee, M.W., 2001. Slow rates of rock surface erosion and sediment production across the Namib Desert and escarpment, Southern Africa. American Journal of Science 301, 326-358.

Bierman, P.R., Caffee, M., 2002. Cosmogenic exposure and erosion history of ancient Australian bedrock landforms. Geological Society of America Bulletin 114, 787-803.

Bierman, P.R., Reuter, J.M., Pavich, M., Gellis, A.C., Caffee, M.W., Larsen, J., 2005. Using cosmogenic nuclides to contrast rates of erosion and sediment yield in a semi-arid, arroyo-dominated landscape, Rio Puerco Basin, New Mexico. Earth Surface Processes and Landforms 30, 935-953.

Boaretto, E., Berkovits, D., Hass, M., Hui, S.K., Kaufman, A., Paul, M., Weiner, S., 2000. Dating of prehistoric caves sediments and flints using ^{10}Be and ^{26}Al in quartz from Tabun Cave (Isreal): Progress report. Nuclear Instruments and Methods in Physics Research B 172, 767-771.

Braun, D., Ron, H., Marco, S., 1991. Magnetostratigraphy of the hominid tool-bearing Erk el Ahmar Formation in the northern Dead Sea Rift. Israel Journal of Earth-Sciences 40, 191-197.

Brown, E.T., Brook, E.J., Raisbeck, G.M., Yiou, F., Kurz, M.D., 1992. Effective attenuation lengths of cosmic rays producing ^{10}Be and ^{26}Al in quartz; implications for exposure age dating. Geophysical Research Letters 19, 369-372.

Carbonell, E., Bermudez de Castro, J.M., Pares, J.M., Perez-Gonzalez, A., Cuenca-Bescos, G., Olle, A., Mosquera, M., Huguet, R., van der Made, J., Rosas, A., Sala, R., Vallverdu, J., Garcia, N., Granger, D.E., Martinon-Torres, M., Rodriguez, X., Stock, G.M., Verges, J.M., Allue, E., Burjachs, F., Caceres, I., Canals, A., Benito, A., Diez, C., Lozano, M., Mateos, A., Navazo, M., Rodriguez, J., Rosell, J., Arsuaga, J.L., 2008. The first hominin of Europe. Nature (London) 452, 465-469.

Chazan, M., Ron, H., Matmon, A., Porat, N., Goldberg, P., Yates, R., Avery, M., Sumner, A., Horwitz, L.K., 2008. Radiometric dating of the Earlier Stone Age sequence in Excavation I at Wonderwerk Cave, South Africa: preliminary results. Journal of Human Evolution 55, 1-11.

Chmeleff, J., von Blanckenburg, F., Kossert, K., Jakob, D., 2010. Determination of the Be-10 half-life by multicollector ICP-MS and liquid scintillation counting. Nuclear Instruments & Methods in Physics Research Section B-Beam Interactions with Materials and Atoms 268, 192-199.

Dunai, T.J., 2000. Scaling factors for production rates of in situ produced cosmogenic nuclides: a critical reevaluation. Earth and Planetary Science Letters 176, 157-169.

Dunai, T.J., 2001. Influence of secular variation of the geomagnetic field on production rates of in situ produced cosmogenic nuclides. Earth and Planetary Science Letters 193, 197-212.

Fink, D., Hotchkis, M., Hua, Q., Jacobsen, G., Smith, A.M., Zoppi, U., Child, D., Mifsud, C., van der Gaast, H., Williams, A., Williams, M., 2004. The ANTARES AMS facility at ANSTO. Nuclear Instruments and Methods in Physics Research B 223-224, 109-115.

Fink, D., Smith, A., 2007. An inter-comparison of ^{10}Be and ^{26}Al AMS reference standards and the ^{10}Be half-life. Nuclear Instruments and Methods in Physics Research, Section B (Beam Interactions with Materials and Atoms) 259, 600-609.

Fruchter, N., 2009. Drainage system evolution of an isolated basin in an arid region: The Makhtesh Hazera as a case study, Earth sciences. Hebrew University, Jerusalem, p. 80.

Gibbon, R.J., Granger, D.E., Kuman, K., Partridge, T.C., 2009. Early Acheulean technology in the Rietputs Formation, South Africa, dated with cosmogenic nuclides. Journal of Human Evolution 56, 152-160.

Ginat, H., Zilberman, E., Saragusti, I., 2003. Early pleistocene lake deposits and Lower Paleolithic finds in Nahal (wadi) Zihor, Southern Negev desert, Israel. Quaternary Research 59, 445-458.

Goethals, M.M., Hetzel, R., Niedermann, S., Wittmann, H., Fenton, C.R., Kubik, P.W., Christl, M., von Blanckenburg, F., 2009. An improved experimental determination of cosmogenic ^{10}Be/^{21}Ne and ^{26}Al/^{21}Ne production ratios in quartz. Earth and Planetary Science Letters 284, 187-198.

Gosse, J.C., Phillips, F.M., 2001. Terrestrial in situ cosmogenic nuclides: theory and application. Quaternary Science Reviews 20, 1475-1560.

Graef, F., Singer, A., Stahr, K. and Jahn, R., 1997. Genesis and diagenesis of Paleosols from Pliocene volcanics on the Golan Heights. Catena 30, 149-167.

Granger, D.E., Kirchner, J.W., Finkel, R.C., 1997. Quaternary downcutting rate of the New River, Virginia, measured from differential decay of cosmogenic ^{26}Al and ^{10}Be in cave-deposited alluvium. Geology 25, 107-110.

Granger, D.E., Smith, A.L., 2000. Dating buried sediments using radioactive decay and muonogenic production of ^{26}Al and ^{10}Be. Nuclear Instruments and Methods in Physics Research B 172, 822-826.

Granger, D.E., Fabel, D., Palmer, A.N., 2001. Pliocene-Pleistocene incision of the Green River, Kentucky, determined from radioactive decay of cosmogenic ^{26}Al and ^{10}Be in Mammoth Cave sediments. Geological Society of America Bulletin 113, 825-836.

Granger, D.E., Muzikar, P.F., 2001. Dating sediment burial with in situ-produced cosmogenic nuclides; theory, techniques, and limitations. Earth and Planetary Science Letters 188, 269-281.

Granger, D.E., 2006. A review of burial dating methods using ^{26}Al and ^{10}Be. Special Paper - Geological Society of America 415, 1-16.

Granger, D.E., Cyr, A.J., Partridge, T.C., 2006. Quantitative tests of cosmogenic nuclide burial dating accuracy. Geochimica et Cosmochimica Acta 70, A212.

Guralnik, B., Matmon, A., Avni, Y., Fink, D., 2010. ^{10}Be exposure ages of ancient desert pavements reveal Quaternary evolution of the Dead Sea drainage basin and rift margin tilting. Earth and Planetary Science Letters 290, 132-141.

Haase-Schramm, A., Goldstein, S.L., Stein, M., 2004. U-Th dating of Lake Lisan (late Pleistocene Dead Sea) aragonite and implications for glacial East Mediterranean climate change. Geochimica et Cosmochimica Acta 68, 985-1005.

Haeuselmann, P., Granger, D.E., Jeannin, P.-Y., Lauritzen, S.-E., 2007. Abrupt glacial valley incision at 0.8 Ma dated from cave deposits in Switzerland. Geology 35, 143-146.

Haviv, I., Enzel, Y., Zilberman, E., Whipple, K., Stone, J., Matmon, A. and Fifield, L.K., 2006b. Climatic control on erosion rates of dolo-limestone hilltops, The Israel Geological Society, Annual Meeting Abstract Book, Bet-Shean, pp. 54.

Heimann, A., Steinitz, G., Mor, D., Shaliv, G., 1996. The Cover Basalt Formation, its age and its regional and tectonic setting; implications from K-Ar and ^{40}Ar/^{39}Ar geochronology. Israel Journal of Earth-Sciences 45, 55-71.

Heisinger, B., Lal, D., Jull, A.J.T., Kubik, P., Ivy-Ochs, S., Knie, K., Nolte, E., 2002a. Production of selected cosmogenic radionuclides by muons: 2. Capture of negative muons. Earth and Planetary Science Letters 200, 357-369.

Heisinger, B., Lal, D., Jull, A.J.T., Kubik, P., S. Ivy-Ochs, S. Neumaier, K. Knie, V. Lazarev, Nolte, E., 2002b. Production of selected cosmogenic radionuclides by muons - 1. Fast muons. Earth and Planetary Science Letters 200, 345-355.

Horowitz, A., 1979. The Quaternary of Israel. Academic Press, New York.

Horowitz, A., 1989. Continuous pollen diagrams for the last 3.5 m.y. from Israel; vegetation, climate and correlation with the oxygen isotope record. Palaeogeography, Palaeoclimatology, Palaeoecology 72, 63-78.

Inbar, N., Shulman, H., Flexer, A., Yellin-Dror, A., 2010. The Structure of Kinnarot Basin, Jordan Rift Valley, Israel, The Israel Geological Society, Annual Meeting Abstract Book, p. 77.

Klein, J., Giegengack, R., Middleton, R., Sharma, P., Underwood, J.R., Weeks, R.A., 1986. Revealing histories of exposure using in situ produced ^{26}Al and ^{10}Be in Libyan desert glass. Radiocarbon 28, 547-555.

Kober, F., Ivy-Ochs, S., Schlunegger, F., Baur, H., Kubik, P.W., Wieler, R., 2007. Denudation rates and a topography-driven rainfall threshold in northern Chile: Multiple cosmogenic nuclide data and sediment yield budgets. Geomorphology 83, 97-120.

Kober, F., Ivy-Ochs, S., Zeilinger, G., Schlunegger, F., Kubik, P.W., Baur, H., Wieler, R., 2009. Complex multiple cosmogenic nuclide concentration and histories in the arid Rio Lluta catchment, northern Chile. Earth Surface Processes and Landforms 34, 398-412.

Kong, P., Granger, D.E., Wu, F.-Y., Caffee, M.W., Wang, Y.-J., Zhao, X.-T., Zheng, Y., 2009. Cosmogenic nuclide burial ages and provenance of the Xigeda paleo-lake: Implications for evolution of the Middle Yangtze River. Earth and Planetary Science Letters 278, 131-141.

Korschinek, G., Bergmaier, A., Faestermann, T., Gerstmann, U.C., Knie, K., Rugel, G., Wallner, A., Dillmann, I., Dollinger, G., von Gostomski, C.L., Kossert, K., Maiti, M., Poutivtsev, M., Remmert, A., 2010. A new value for the half-life of ^{10}Be by Heavy-Ion Elastic Recoil Detection and liquid scintillation counting. Nuclear Instruments & Methods in Physics Research Section B-Beam Interactions with Materials and Atoms 268, 187-191.

Lourens, L., Hilgen, F.J., Shackleton, N.J., Laskar, J., Wilson, D., 2004. Orbital tuning calibrations and conversions for the Neogene period. Cambridge University Press, Cambridge, United Kingdom, pp. 469-484.

Marcus, E., Slager, J., 1985. The sedimentary-magmatic sequence of the Zemah 1 well (Jordan-Dead Sea Rift, Israel) and its emplacement in time and space. Israel Journal of Earth-Sciences 34, 1-10.

Martinez-Navarro, B., Belmaker, M., Bar-Yosef, O., 2009. The large carnivores from 'Ubeidiya (early Pleistocene, Israel): biochronological and biogeographical implications. Journal of Human Evolution 56, 514-524.

Matmon, A., Crouvi, O., Enzel, Y., Bierman, P., Larsen, J., Porat, N., Amit, R., Caffee, M., 2003. Complex exposure histories of chert clasts in the late Pleistocene shorelines of Lake Lisan, southern Israel. Earth Surface Processes and Landforms 28, 493–506.

Matmon, A., Schwartz, R., Finkel, R.C., Clemmens, S., Hanks, T., 2005. Dating offset fans along the Mojave section of the San Andreas Fault using cosmogenic ^{26}Al and ^{10}Be Geological Society of American Bulletin 117, doi: 10.1130/B25590.25591.

Matmon, A., Simhai, O., Amit, R., Haviv, I., Porat, N., McDonald, E., Benedetti, L., Finkel, R., 2009. Desert pavement-coated surfaces in extreme deserts present the longest-lived landforms on Earth. Bulletin of the Geological Society of America 121, 688-697.

Niedermann, S., Graf, T., Kim, J.S., Kohl, C.P., Marti, K., Nishiizumi, K., 1994. Cosmic-ray-produced ^{21}Ne in terrestrial quartz: the neon inventory of Sierra Nevada quartz separates. Earth and Planetary Science Letters 125, 341-355.

Niedermann, S., Bach, W., Erzinger, J., 1997. Noble gas evidence for a lower mantle component in MORBs from the southern East Pacific Rise: decoupling of helium and neon isotope systematics. Geochimica et Cosmochimica Acta 61, 2697-2715.

Niedermann, S., 2000. The ^{21}Ne production rate in quartz revisited. Earth and Planetary Science Letters 183, 361-364.

Niedermann, S., 2002. Cosmic-ray-produced noble gases in terrestrial rocks; dating tools for surface processes. Reviews in Mineralogy and Geochemistry 47, 731-784.

Nishiizumi, K., Winterer, E.L., Kohl, C.P., Klein, J., Middleton, R., Lal, D., Arnold, J.R., 1989. Cosmic ray production rates of ^{10}Be and ^{26}Al in quartz from glacially polished rocks. Journal of Geophysical Research, B, Solid Earth and Planets 94, 17,907-917,915.

Nishiizumi, K., Kohl, C.P., Arnold, J.R., Dorn, R., Klein, J., Fink, D., Middleton, R., Lal, D., 1993. Role of in situ cosmogenic nuclides ^{10}Be and ^{26}Al in the study of diverse geomorphic processes. Earth Surface Processes and Landforms 18, 407-425.

Nishiizumi, K., 2004. Preparation of ^{26}Al AMS standards. Nuclear Instruments and Methods in Physics Research B 223-224, 388-392.

Nishiizumi, K., Imamura, M., Caffee, M.W., Southon, J.R., Finkel, R.C., McAninch, J., 2007. Absolute calibration of ^{10}Be AMS standards. Nuclear Instruments and Methods in Physics Research, Section B 258, 403-413.

Ogg, J.G., Smith, A.G., 2004. The geomagnetic polarity time scale, A Geologic Time Scale 2004. Cambridge University Press, Cambridge, United Kingdom, pp. 63-86.

Opdyk, N.D., Channell, J.E.T., 1996. Magnetic Stratigraphy. Academic Press.

Partridge, T.C., Granger, D.E., Caffee, M.W., Clarke, R.J., 2003. Lower Pliocene Hominid Remains from Sterkfontein. Science 300, 607-612.

Picard, L., 1965. The geological evolution of the Quaternary in the central-northern Jordan graben, Israel. Geological Society of America, Special paper 84, 337-366.

Placzek, C.J., Matmon, A., Granger, D.E., Quade, J., Niedermann, S., Evidence for active landscape evolution in the hyperarid Atacama from multiple terrestrial cosmogenic nuclides. Earth and Planetary Science Letters 295, 12-20.

Reed, B.C., 1989. Linear least-squares fits with errors in both coordinates. American Journal of Physics 57, 642-646.

Repka, J.L., Anderson, R.S., Finkel, R.C., 1997. Cosmogenic dating of fluvial terraces, Fremont River, Utah. Earth and Planetary Science Letters 152, 59-73.

Ron, H., Levi, S., 2001. When did hominids first leave Africa? New high-resolution magnetostratigraphy from the Erk-el-Ahmar formation, Israel. Geology 29, 887-890.

Rood, D.H., Hall, S., Guilderson, T.P., Finkel, R.C., Brown, T.A., 2010. Challenges and opportunities in high-precision ^{10}Be measurements at CAMS. Nuclear Instruments and Methods in Physics Research Section B: Beam Interactions with Materials and Atoms 268, 730-732.

Rotstein, Y., Bartov, Y., Frieslander, U., 1992. Evidence for local shifting of the main fault and changes in the structural setting, Kinarot Basin, Dead Sea Transform. Geology 20, 251-254.

Sadler, P.M., 1981. Sediment accumulation rates and the completeness of stratigraphic sections. Journal of Geology 89, 569-584.

Safran, E.B., Bierman, P.R., Aalto, R., Dunne, T., Whipple, K.X., Caffee, M., 2005. Erosion rates driven by channel network incision in the Bolivian Andes. Earth Surface Processes and Landforms 30, 1007-1024.

Schütt, H., Ortal, R., 1993. A preliminary correlation between the plio-pleistocene malacofaunas of the Jordan Valley (Israel) and the Orontes Valley (Syria). Zoology in the Middle East 8, 69-111.

Schulman, N., 1959. The geology of the central Jordan valley. Bulletin of the Research Council of Israel, Section G: Geo-Sciences 8, 63-90.

Shaliv, G., 1991. Stages in the tectonic and volcanic history of Neogen continental basins in northern Israel. Geological Survey of Israel, report GSI/11/91, p. 94.

Shen, G., Xing, G., Bin, G., Granger, D.E., 2009. Age of Zhoukoudian Homo erectus determined with ^{26}Al/^{10}Be burial dating. Nature (London) 458, 198-200.

Shuster, D.L., Farley, K.A., 2005. Diffusion kinetics of proton-induced ^{21}Ne, ^{3}He, and ^{4}He in quartz. Geochimica et Cosmochimica Acta 69, 2349-2359.

Siedner, G., Horowitz, A., 1974. Radiometric ages of late Cainozoic basalts from northern Israel: chronostratigraphic implications. Nature 250, 23-26.

Singer, A., 2007. The Soils of Israel. Springer, 306 pp.

Stock, G.M., Anderson, R.S., Finkel, R.C., 2004. Pace of landscape evolution in the Sierra Nevada, California, revealed by cosmogenic dating of cave sediments. Geology 32, 193-196.

Stone, J., 2000. Air pressure and cosmogenic isotope production. Journal of Geophysical Research 105, 23753-23759.

Tchernov, E., 1975. The Early Pleistocene Molluscs of 'Erk el-Ahmar', The Pleistocene of the central Jordan valley, The excavations at 'Ubbeidiya'. The Israel academy of sciences and humanities, Jerusalem, p. 36.

Tchernov, E., Guerin, C., Ballesio, R., Bar-Yosef, O., Beden, M., Eisenmann, V., Faure, M., Geraads, D., Volokita, M., 1986. Conclusion sur la faune du gisement pléistocène ancien d'Oubeidiyeh (Israel); implications paléoécologiques, biogéographiques et stratigraphiques: Memoires et Travaux du Centre de Recherches Préhistoriques Français de Jérusalem 5, 351-398.

Tchernov, E., 1987. The age of the 'Ubeidiya Formation, an early Pleistocene hominid site in the Jordan Valley, Israel. Israel Journal of Earth-Sciences 36, 3-30.

Vermeesch, P., Fenton, C.R., Kober, F., Wiggs, G.F.S., Bristow, C.S., Xu, S., Sand residence times of one million years in the Namib Sand Sea from cosmogenic nuclides. Nature Geoscience 3, 862-865.

Wolkowinsky, A.J., Granger, D.E., 2004. Early Pleistocene incision of the San Juan River, Utah, dated with ^{26}Al and ^{10}Be. Geology 32, 749-752.

Zilberman, E., Begin, Z.B., 1997. Main stages and rate of the relief development in Israel. Geological Survey of Israel, Report GSI/24/97, p. 52.

Figure 1:

A) General location of the study area in the eastern Mediterranean.

B) Digital elevation image of the study area showing the study site south of Lake Kinneret (Sea of Galilee) at the western margin of the Dead Sea rift valley.

C) Exposed lacustrine section of the Erk-el-Ahmar Formation along the bank of the Jordan River. The section is tilted down to the east and the layers in the foreground dip under the layers in the background. The section is eroded horizontally on the top. The resultant erosional surface is marked with a black horizontal line. Sample locations are marked on the photo. (Sample 7a and 9 are not marked and were collected further up section, behind the cliff in the background). Samples 1a to 1d belong to the same stratigraphic layer

Figure 2:

Three-isotope plot showing the stepwise heating data for samples EEA-1b and EEA-2. See text for cosmogenic ^{21}Ne calculations. Dotted line labeled “mfl” is the mass fractionation line of air. The 1200°C step of EEA-1b lies far to the right and appears in inset. Uncertainties of 1σ are marked.

Figure 3:

A) ^{26}Al-^{10}Be exposure-burial plot of EEA samples with 68% confidence ellipses (see text for parameters used for the plot). Calculated pre-burial concentrations of quartz and chert end members are plotted including the expected locus (^{26}Al/^{10}Be ratio vs ^{10}Be concentration) which results from mixing them at different ratios (10% intervals are marked). The mixing causes a maximum $^{26}Al/^{10}Be$ ratio depression equivalent to ~0.5 Ma burial at 30% chert: 70% quartz.

B) Inset showing an expanded view of the EEA samples. A mixing line based on the linear fitting of ^{26}Al and ^{10}Be concentrations vs. chert content for samples EEA-1(a-d) to 4 (see text and Fig. 5B) is added. Also shown, are the expected concentrations and uncertainties of both end members, based on this fitting. Burial ages of samples EEA-6, 7a, and 9 are corrected based on their distance from the mixing line which represents a weighted mean age of 4.5±0.6 Ma (Table 3). The pre-burial quartz-chert mixing line in fig 3A is calculated by back calculating 4.5 Ma from the mixing line in B.

Figure 4:

^{10}Be-^{21}Ne and ^{26}Al-^{21}Ne exposure-burial plots for two samples from the Erk-el-Ahmar formation.

Figure 5:

A) Quartz and chert grains seen under a polarizing microscope.

B) ^{10}Be and ^{26}Al concentrations vs. chert fraction in sample. ^{26}Al and ^{10}Be of samples from the bottom 6 m of the section (EEA-1 to EEA-4; triangles) plot on a mixing line. All other samples (EEA-5, 6, 7a, and 9; open diamonds) plot above the mixing lines. In the ^{26}Al plot sample EEA-3 plots below the fitted line. Regression lines for the mixing were computed using linear least-squares fits with errors in both coordinates (Reed, 1989). ^{10}Be uncertainties are equal or smaller than the size of the symbols.

Figure 6:

Two possible correlations of the Erk-el-Ahmar section to the magnetic polarity timescale (Lourens et al., 2004; Ogg and Smith, 2004) using magnetostratigraphy and cosmogenic burial ages. Dashed parts of the magnetic section have unknown magnetic polarity due to debris cover. Corrected cosmogenic nuclide ages with 1σ uncertainties (Table 3) are placed on the time scale to the right as labeled bars (samples EEA-3 and EEA-5 are omitted due to very large uncertainties). Correlations A and B differ only by the different interpretation of the reversal at the bottom of the section. Option A is less probable than B as it overlaps with the older ‘Cover Basalt’ formation.

[1]Braun et al., 1991, [2]Ron and Levi, 2001, [3]This study

Table 1:

Sample data, AMS analytical data, and ^{10}Be and ^{26}Al concentrations with 1σ uncertainties

Site location: 32.636°N 35.560°E.

Site altitude (at erosional surface): 210±10 m below sea level.

[a] Measured at ANSTO. ^{10}Be/^{9}Be normalized to SRM4235 = 2.79×10^{-11}.

^{26}Al/^{27}Al normalized to Vogt SRM Z92-0221 = 1.68×10^{-11}.

[b] Measured at LLNL. ^{10}Be/^{9}Be normalized to 07KNSTD3110 = 2.85×10^{-12}

^{26}Al/^{27}Al normalized to KNSTD 10650 = 1.065×10^{-11}.

[c] In parentheses – extrapolated depth below erosional surface (see Fig. 1).

Table 2:

^{21}Ne excesses (relative to atmospheric isotopic composition, in units of 10^5 atoms/g) as determined by stepwise heating. See text for derivation of the assumed total cosmogenic ^{21}Ne concentrations. Uncertainties are 1σ.

Table 3:

Calculated burial ages for the Erk-el-Ahmar formation samples

[a] Assuming simple exposure-burial history with insignificant post burial production. Age uncertainties are based on the analytical uncertainties (minimum to maximum $^{26}Al/^{10}Be$ ratio).

[b] Assuming samples EEA1-4 are of similar age, correction is based on end member ages derived from fitting chert-quartz mixing ratios to concentrations (Fig. 3B,5B). Ages of samples EEA-6, EEA-7a, and EEA-9 are corrected based on their distance from the mixing line (Fig. 3B)

[c] Best correlation based on magnetostratigraphy and geological constraints (Fig. 6 and text)

[d] Sample EEA-3 lies in the forbidden zone (Fig. 3B).

Figure 1

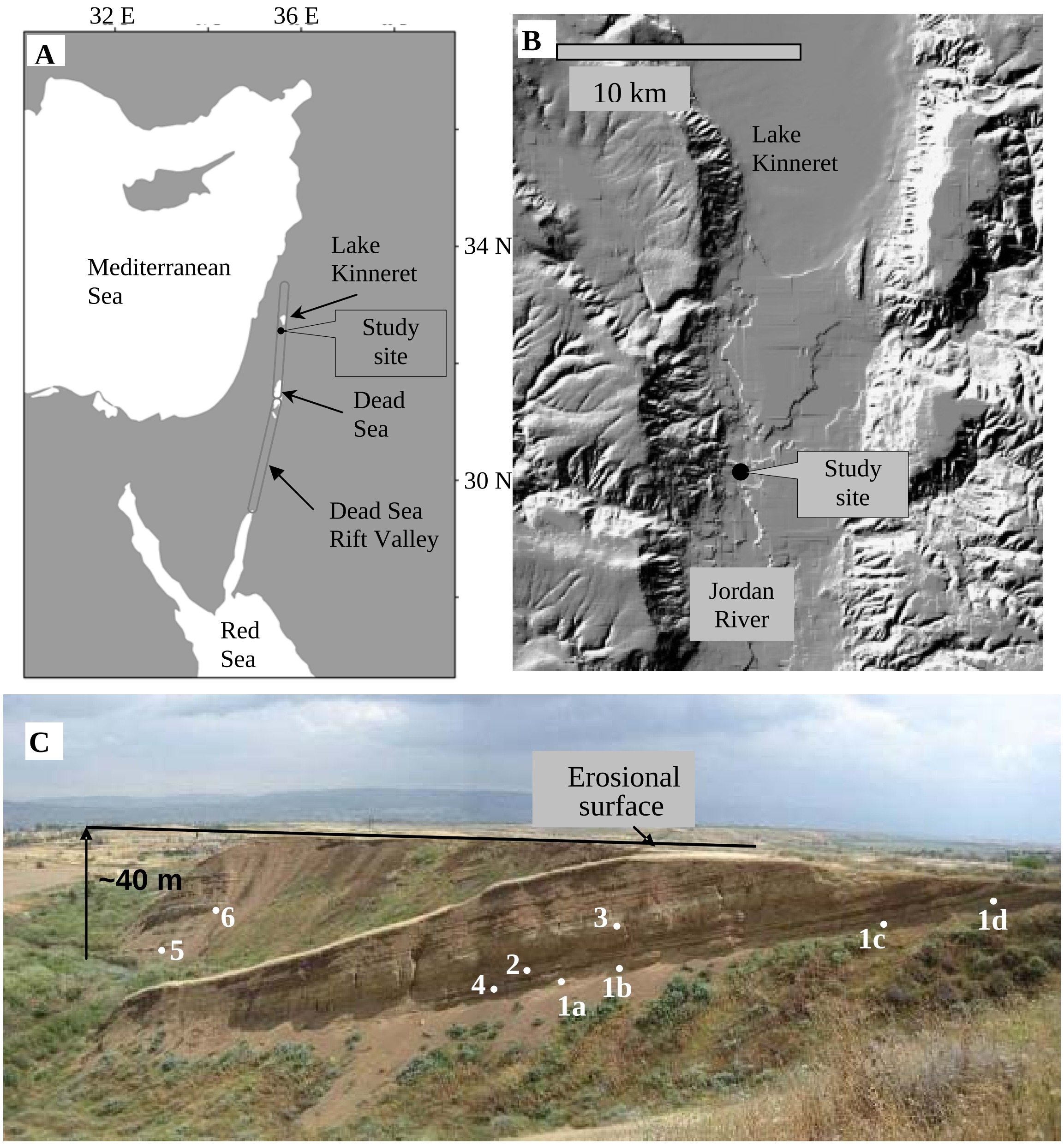

A
32 E
36 E
34 N
30 N
Mediterranean Sea
Lake Kinneret
Study site
Dead Sea
Dead Sea Rift Valley
Red Sea
B
10 km
Lake Kinneret
Study site
Jordan River
C
Erosional surface
~40 m
6
5
3
2
4
1a
1b
1c
1d

Figure 2

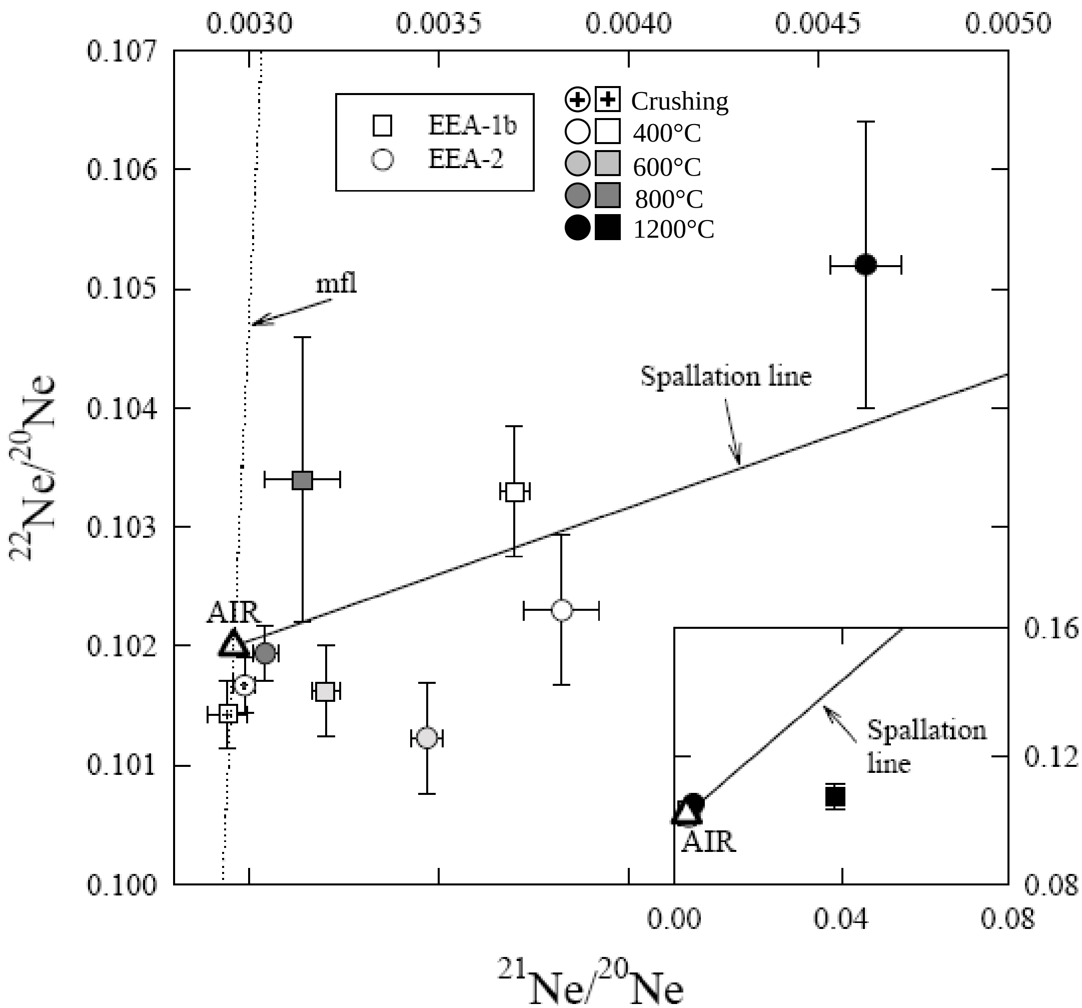

0.0030
0.0035
0.0040
0.0045
0.0050
0.107
0.106
0.105
0.104
0.103
0.102
0.101
0.100
EEA-1b
EEA-2
Crushing
400°C
600°C
800°C
1200°C
mfl
Spallation line
AIR
Spallation
line
AIR
0.16
0.12
0.08
0.00
0.04
0.08
^{22}Ne/^{20}Ne
^{21}Ne/^{20}Ne

Figure 3

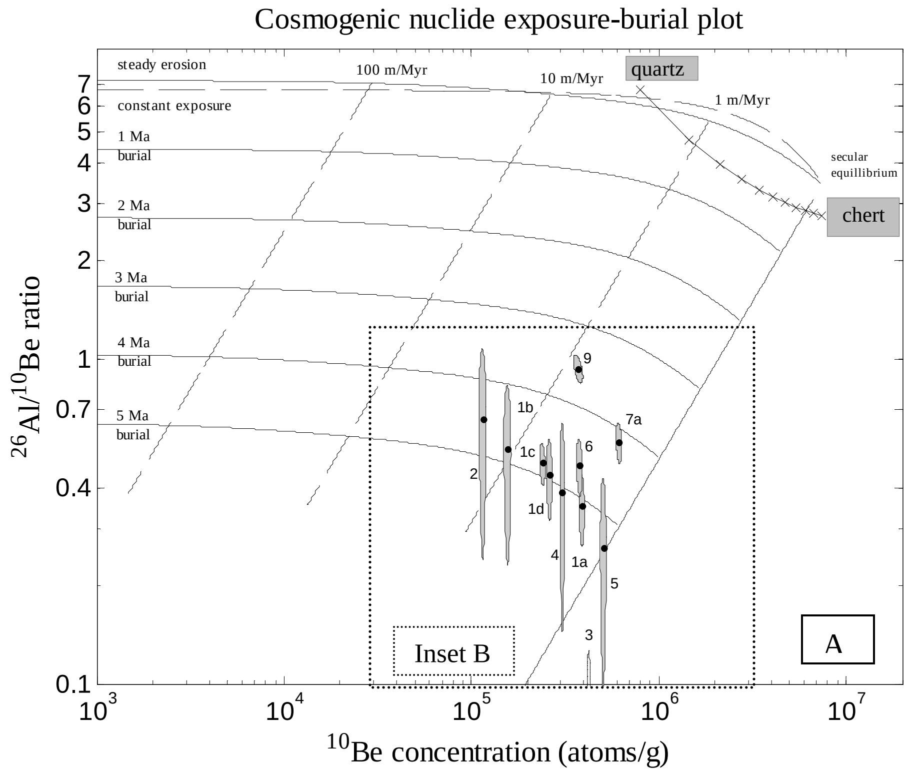

Cosmogenic nuclide exposure-burial plot
steady erosion
100 m/Myr
10 m/Myr
quartz
1 m/Myr
constant exposure
1 Ma burial
2 Ma burial
3 Ma burial
4 Ma burial
5 Ma burial
secular equillibrium
chert
Inset B
A
$^{26}Al/^{10}Be$ ratio
^{10}Be concentration (atoms/g)

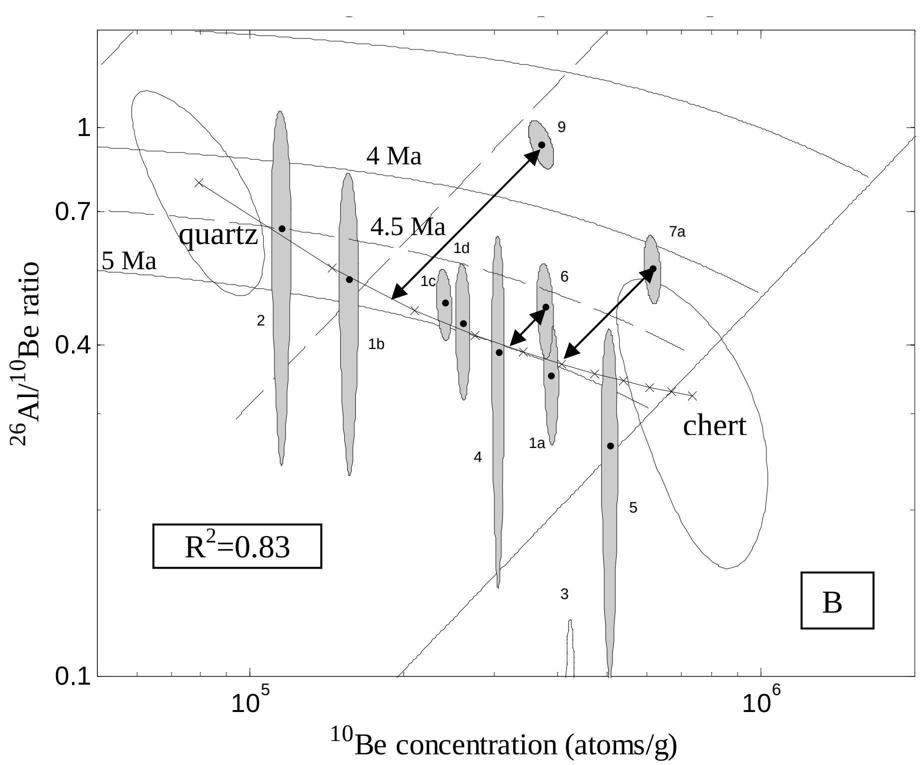

4 Ma
4.5 Ma
5 Ma
quartz
chert
R^2=0.83
B
$^{26}Al/^{10}Be$ ratio
^{10}Be concentration (atoms/g)

Figure 4

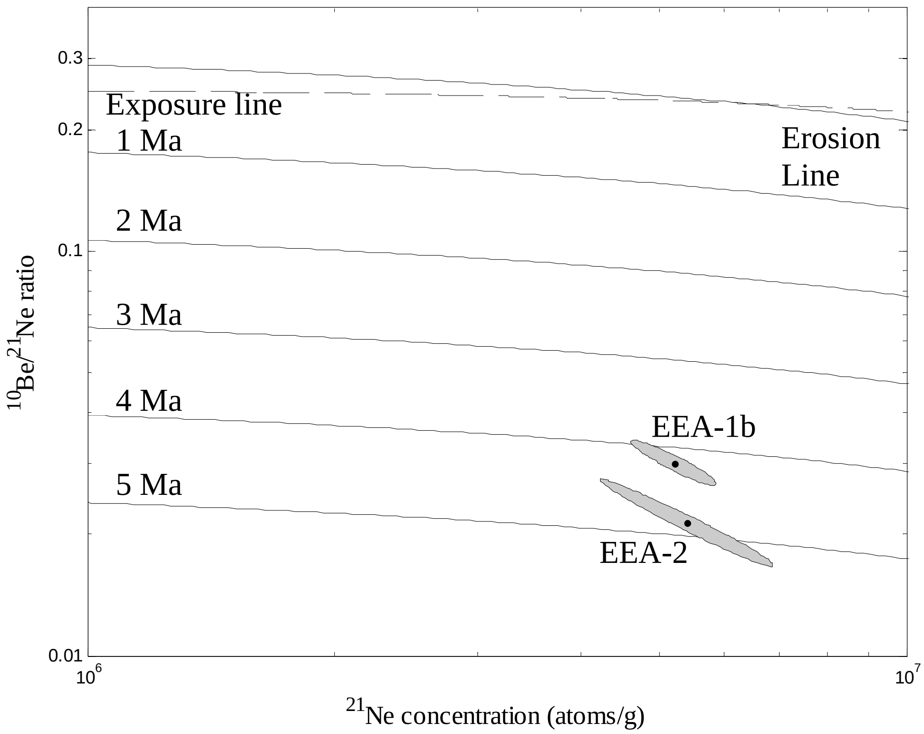
0.3
0.2
0.1
0.01
Exposure line
1 Ma
2 Ma
3 Ma
4 Ma
5 Ma
Erosion
Line
EEA-1b
EEA-2
10Be/21Ne ratio
10^6
10^7
21Ne concentration (atoms/g)

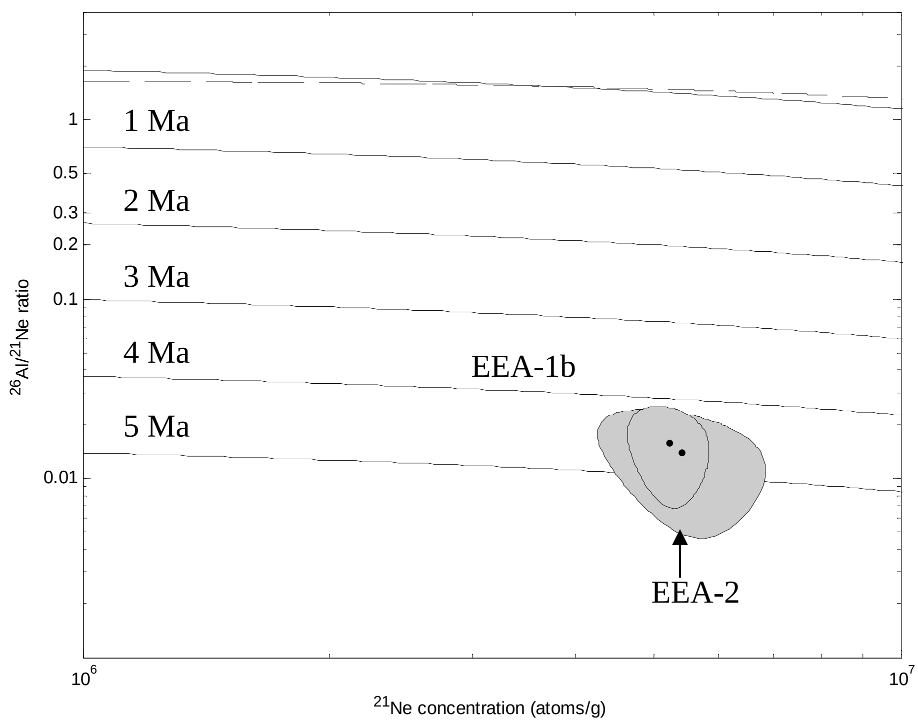
1
0.5
0.3
0.2
0.1
0.01
1 Ma
2 Ma
3 Ma
4 Ma
5 Ma
EEA-1b
EEA-2
26Al/21Ne ratio
10^6
10^7
21Ne concentration (atoms/g)

Figure 5

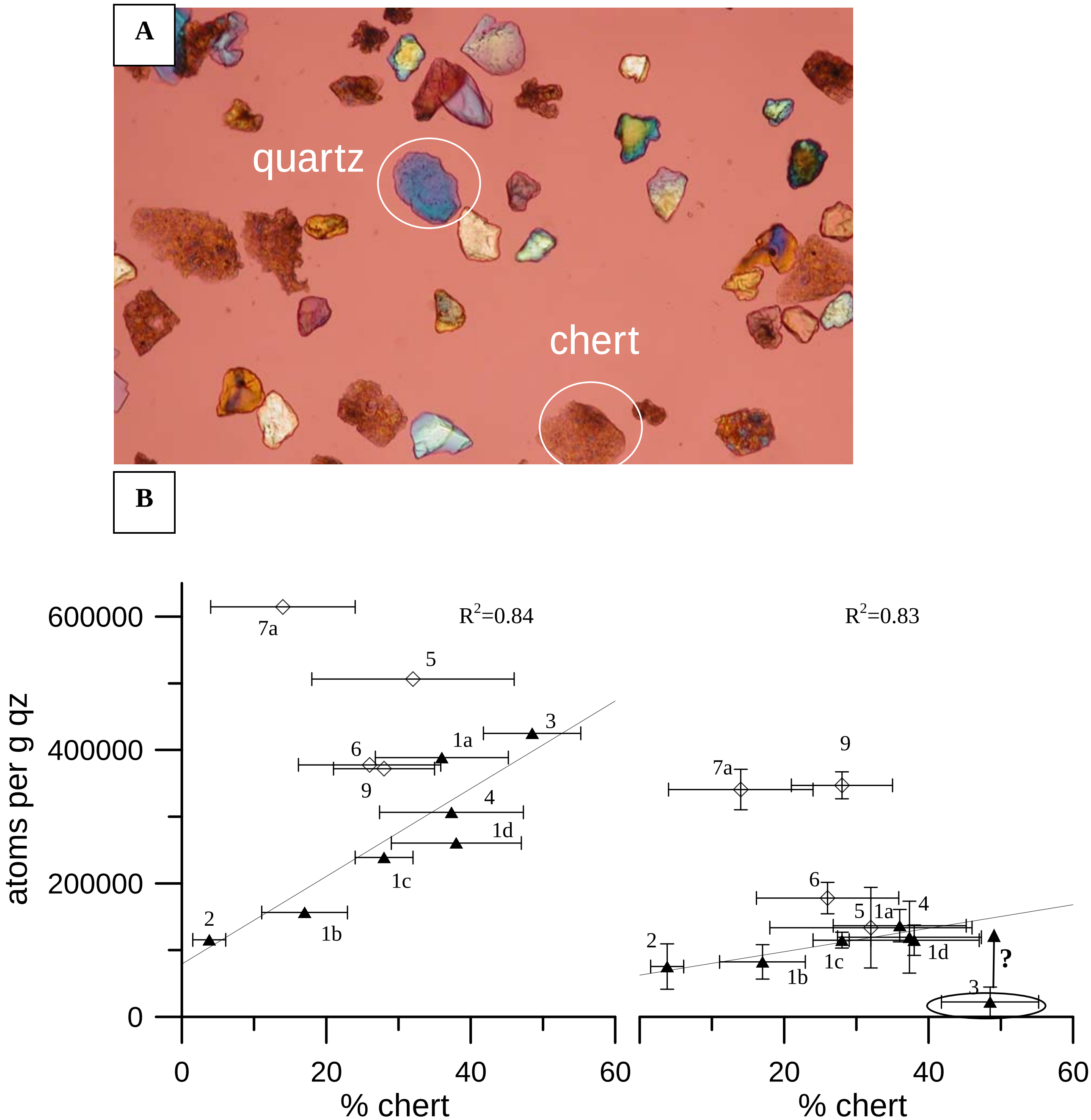

$^{10}Be = 6570 \times \%chert + 79140$

$^{26}Al = 1756 \times \%chert + 62670$

Figure 6

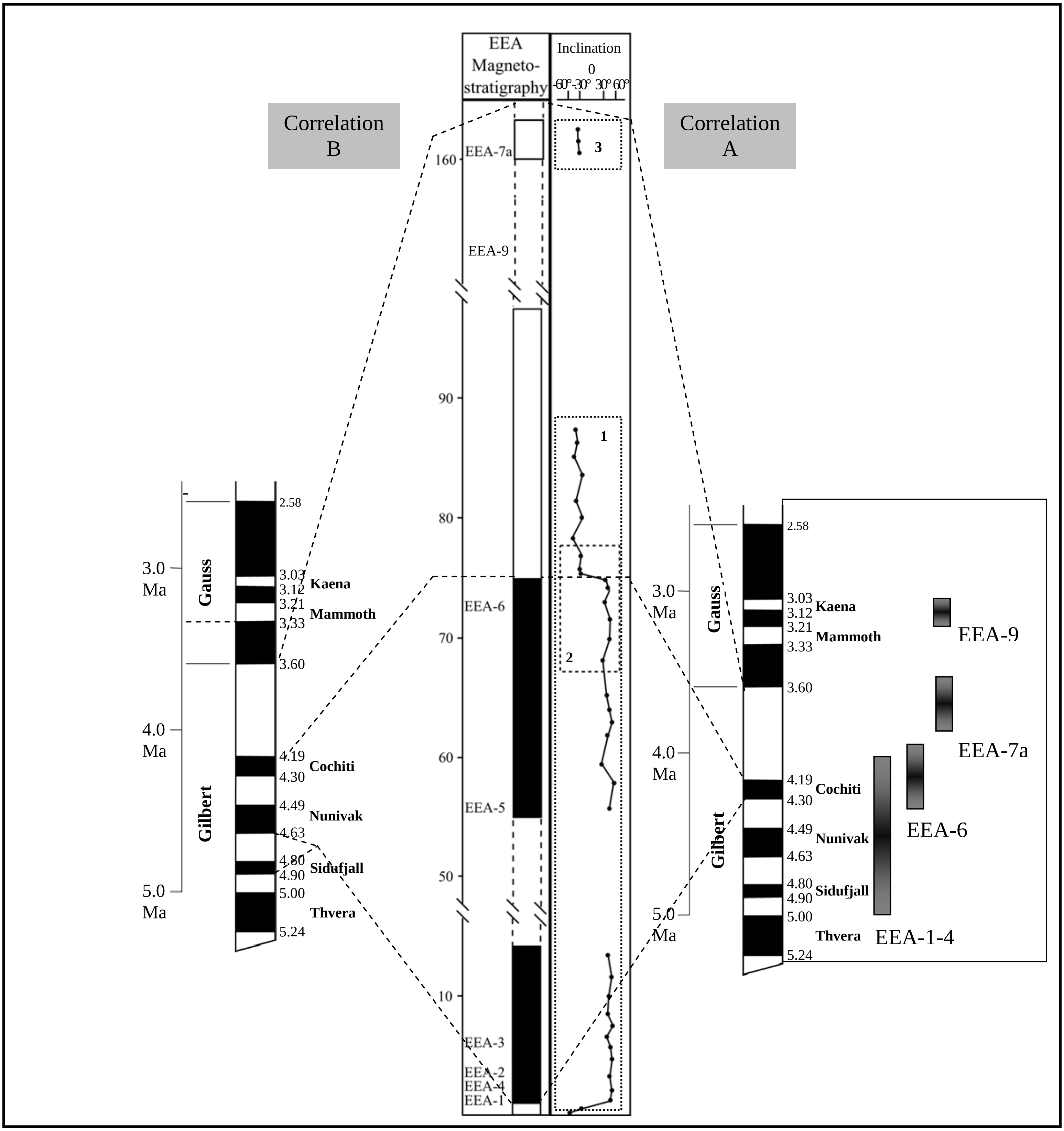

EEA Magneto-stratigraphy
Inclination
0
-60° -30° 30° 60°
Correlation B
Correlation A
EEA-7a
160
EEA-9
90
80
70
60
50
10
EEA-6
EEA-5
EEA-3
EEA-2
EEA-4
EEA-1
1
2
3
3.0 Ma
4.0 Ma
5.0 Ma
Gauss
Gilbert
2.58
3.03
3.12
3.21
3.33
3.60
4.19
4.30
4.49
4.63
4.80
4.90
5.00
5.24
Kaena
Mammoth
Cochiti
Nunivak
Sidufjall
Thvera
EEA-9
EEA-7a
EEA-6
EEA-1-4

Table 1

Sample	AMS std	Burial depth[c] [m]	quartz [g]	Be carrier [mg]	Al carrier [mg]	$^{10}Be/^{9}Be$ [×10^{-15}]	^{10}Be [10^{5} atoms g^{-1}]	Stable Al [×10^{18} atoms g^{-1}]	$^{26}Al/^{27}Al$ [10^{-15}]	^{26}Al [10^{5} atoms g^{-1}]	$^{26}Al/^{10}Be$	^{21}Ne [10^{5} atoms g^{-1}]
EEA-1a	b	14 (16)	40.000	0.298	0	780±18	3.88 ± 0.10	4.50±0.09	30.4±5.4	1.37 ± 0.24	0.35 ± 0.06	
EEA-1b	a	14	35.153	0.300	0.297	274±8	1.57 ± 0.05	3.34±0.10	25±10	0.83 ± 0.33	0.53 ± 0.21	52.0 ± 4.3
EEA-1c	b	4.5	35.012	0.296	0	423±10	2.39 ± 0.06	3.78±0.04	30.4±3.1	1.15 ± 0.12	0.48 ± 0.05	
EEA-1d	b	2	35.013	0.295	0	462±11	2.61 ± 0.06	3.75±0.09	30.7±6.0	1.15 ± 0.22	0.44 ± 0.09	
EEA-2	a	12.5 (14)	35.010	0.298	0.297	203±6	1.16 ± 0.04	3.81±0.11	20±9	0.75 ± 0.34	0.65 ± 0.30	54 ± 9
EEA-3	a	8.5	32.181	0.301	0.099	678±12	4.24 ± 0.12	7.57±0.23	3±3	0.23 ± 0.23	0.05 ± 0.05	
EEA-4	a	12 (16)	40.854	0.294	0	635±13	3.07 ± 0.18	4.12±0.12	29±13	1.19 ± 0.53	0.39 ± 0.18	
EEA-5	a	36	25.114	0.300	0.098	634±16	5.07 ± 0.13	12.2±0.4	11±5	1.34 ± 0.60	0.26 ± 0.12	
EEA-6	b	21	35.067	0.287	0	691±17	3.78 ± 0.10	5.83±0.43	30.6±4.0	1.78 ± 0.23	0.47 ± 0.06	
EEA-7a	b	36	40.067	0.298	0	1233±29	6.14 ± 0.16	6.07±0.15	56.1±5.0	3.41 ± 0.30	0.55 ± 0.05	
EEA-9	b	30	35.006	0.293	0	663±27	3.72 ± 0.15	3.29±0.06	105±6	3.47 ± 0.20	0.93 ± 0.07	

Table 2

Temp.	EEA-1b	EEA-2
400°C	32.7±2.0	6.3±0.8
600°C	18.1±2.8	41.7±3.8
800°C	$2.4^{+1.4}/_{-1.2}$	12.6±5.0
1200°C	20.3±1.1	17.8±1.1
Total 400-800°C	53.2±3.7	61±7
Total 400-600°C	50.8±3.4	48.0±3.8
Assumed cosmogenic ^{21}Ne	52.0±4.3	54±9

Table 3

Sample	Burial age [Ma] [a]			Corrected burial age [Ma] [b]	Paleomagnetic correlated burial ages [Ma] [c]
	^{26}Al-^{10}Be	^{21}Ne-^{10}Be	^{21}Ne-^{26}Al		
EEA-1a	$5.09^{+0.32}_{-0.28}$			4.5±0.6	4.30
EEA-1b	$4.85^{+0.91}_{-0.66}$	4.06±0.18	4.49±0.42		
EEA-1c	$4.85^{+0.22}_{-0.20}$				
EEA-1d	$4.95^{+0.39}_{-0.33}$				
EEA-2	$4.54^{+1.12}_{-0.75}$	4.73±0.34	4.61±0.49		
EEA-3	N/A [d]			[d]	
EEA-4	$5.07^{+0.92}_{-0.62}$			4.5±0.6	
EEA-5	$5.3^{+1}_{-0.6}$			$5.0^{+1}_{-0.6}$	4.19-4.30
EEA-6	$4.67^{+0.27}_{-0.24}$			4.2±0.3	4.19
EEA-7a	$4.16^{+0.19}_{-0.18}$			3.7±0.2	3.60-4.19
EEA-9	$3.58^{+0.16}_{-0.17}$			3.15±0.17	3.60-4.19